nature neuroscience

Surface diffusion of astrocytic glutamate transporters shapes synaptic transmission

Ciaran Murphy-Royal[1–3], Julien P Dupuis[2,3], Juan A Varela[2,3,6], Aude Panatier[1,2,6], Benoît Pinson[2,4], Jérôme Baufreton[2,5], Laurent Groc[2,3,7] & Stéphane H R Oliet[1,2,7]

Control of the glutamate time course in the synapse is crucial for excitatory transmission. This process is mainly ensured by astrocytic transporters, high expression of which is essential to compensate for their slow transport cycle. Although molecular mechanisms regulating transporter intracellular trafficking have been identified, the relationship between surface transporter dynamics and synaptic function remains unexplored. We found that GLT-1 transporters were highly mobile on rat astrocytes. Surface diffusion of GLT-1 was sensitive to neuronal and glial activities and was strongly reduced in the vicinity of glutamatergic synapses, favoring transporter retention. Notably, glutamate uncaging at synaptic sites increased GLT-1 diffusion, displacing transporters away from this compartment. Functionally, impairing GLT-1 membrane diffusion through cross-linking *in vitro* and *in vivo* slowed the kinetics of excitatory postsynaptic currents, indicative of a prolonged time course of synaptic glutamate. These data provide, to the best of our knowledge, the first evidence for a physiological role of GLT-1 surface diffusion in shaping synaptic transmission.

Glutamate is the major excitatory transmitter in the CNS. At the majority of glutamate synapses in the forebrain, neurotransmitter clearance is ensured by GLT-1, a highly specific glutamate transporter that is expressed on astrocytes[1]. Each quantal event is believed to result in the release of 4,000 molecules of glutamate[2], transiently increasing the concentration of this neurotransmitter to 1 mM before returning to basal concentrations[3]. As there are no extracellular enzymes to degrade glutamate, this brief transient can only be attributed to the diffusion of glutamate in the extracellular space combined with its efficient uptake by transporters. Taking into consideration the slow transport cycle of this family of transporters (from 12 to 70 ms per cycle)[4,5], relative to the time course of glutamate in the synaptic cleft[3], it has been hypothesized that thousands of transporters must be present near synapses to efficiently remove this neurotransmitter on a rapid timescale[6,7]. Given that glutamate transporters and receptors have similar affinities for glutamate[8], it is currently believed that transporters curtail receptor activation by effectively competing for glutamate at the synapse, thereby maintaining point-to-point transmission and preventing excitotoxic neuronal cell death[9].

The molecular mechanisms regulating intracellular trafficking, endocytosis and exocytosis, and surface expression of GLT-1 have been under high scrutiny[10–13], as these processes are likely important in synaptic physiology. Although the role of glutamate transporters in controlling the time course of synaptic glutamate[14–16] and limiting heterosynaptic spillover[17,18] has been clearly defined, evidence for a contribution of GLT-1 surface trafficking in the physiological regulation of glutamatergic neurotransmission remains unexplored.

It was recently demonstrated that glutamatergic neurotransmission is partly regulated by lateral diffusion of receptors on hippocampal neurons[19]. In addition, surface trafficking of receptors is not solely a neuronal phenomenon, but also occurs on glial cells[20,21]. Thus, we hypothesized that surface diffusion of GLT-1 on astrocytes could contribute to the regulation of excitatory neurotransmission. We found that GLT-1 diffused on the surface of astrocytes in an activity-dependent manner. By recording neuronal activity in cultures and in hippocampal brain slices while immobilizing GLT-1, we implicate surface diffusion of GLT-1 in the physiological regulation of the time course of synaptic glutamate *in vitro* and *in vivo*. Our results indicate that surface diffusion of the glutamate transporter GLT-1 has an active role in shaping glutamate transmission in synapses, likely through providing sufficient numbers of transporters to compete with receptors for synaptically released glutamate.

RESULTS

GLT-1 is highly mobile on the surface of astrocytes

We employed a GLT-1 transporter with a flag tag (DYKDDDDK) inserted into the second extracellular loop of the protein (GLT-1^{flag}; **Supplementary Fig. 1a**). Using radio-labeled glutamate, we first confirmed that the transport function of GLT-1^{flag} expressed in COS-7 cells and mixed primary hippocampal cultures was not affected by the insertion of this flag tag (**Fig. 1a**). To observe surface diffusion of GLT-1 in live hippocampal cultures and explore its behavior in synaptic areas, we used a single nanoparticle (quantum dot, QD) tracking technique. Single nanoparticle imaging provides, among others, two

[1]Neurocentre Magendie, Inserm U862, Bordeaux, France. [2]University of Bordeaux, Bordeaux, France. [3]Interdisciplinary Institute for Neuroscience, CNRS UMR 5297, Bordeaux, France. [4]Institute for Biochemistry and Cellular Genetics, CNRS UMR 5095, Bordeaux, France. [5]Institute of Neurodegenerative Diseases, CNRS UMR 5293, Bordeaux, France. [6]These authors contributed equally to this work. [7]These authors jointly directed this work. Correspondence should be addressed to L.G. (laurent.groc@u-bordeaux2.fr) or S.H.R.O. (stephane.oliet@inserm.fr).

Received 1 August 2014; accepted 14 November 2014; published online 12 January 2015; doi:10.1038/nn.3901

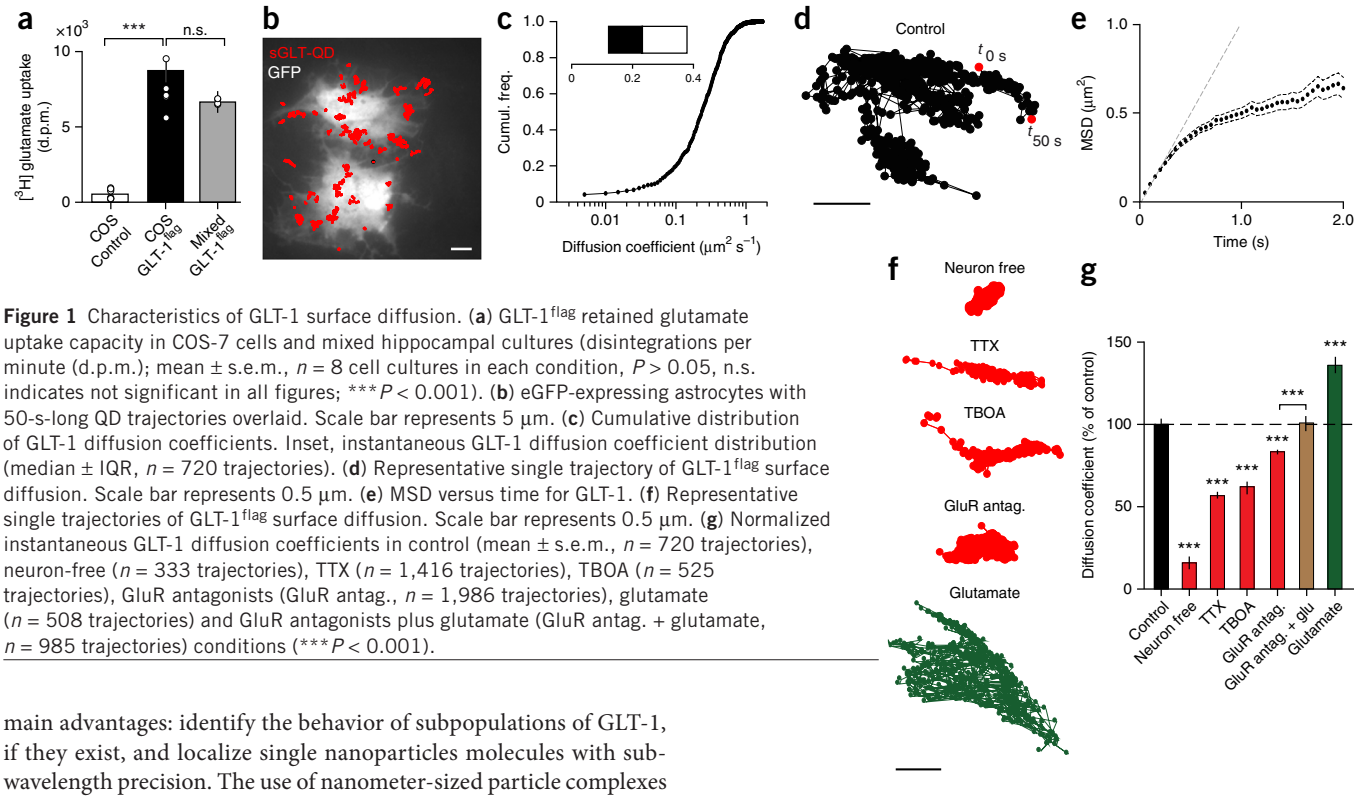

Figure 1 Characteristics of GLT-1 surface diffusion. (**a**) GLT-1^{flag} retained glutamate uptake capacity in COS-7 cells and mixed hippocampal cultures (disintegrations per minute (d.p.m.); mean ± s.e.m., $n = 8$ cell cultures in each condition, $P > 0.05$, n.s. indicates not significant in all figures; $^{***}P < 0.001$). (**b**) eGFP-expressing astrocytes with 50-s-long QD trajectories overlaid. Scale bar represents 5 μm. (**c**) Cumulative distribution of GLT-1 diffusion coefficients. Inset, instantaneous GLT-1 diffusion coefficient distribution (median ± IQR, $n = 720$ trajectories). (**d**) Representative single trajectory of GLT-1^{flag} surface diffusion. Scale bar represents 0.5 μm. (**e**) MSD versus time for GLT-1. (**f**) Representative single trajectories of GLT-1^{flag} surface diffusion. Scale bar represents 0.5 μm. (**g**) Normalized instantaneous GLT-1 diffusion coefficients in control (mean ± s.e.m., $n = 720$ trajectories), neuron-free ($n = 333$ trajectories), TTX ($n = 1{,}416$ trajectories), TBOA ($n = 525$ trajectories), GluR antagonists (GluR antag., $n = 1{,}986$ trajectories), glutamate ($n = 508$ trajectories) and GluR antagonists plus glutamate (GluR antag. + glutamate, $n = 985$ trajectories) conditions ($^{***}P < 0.001$).

main advantages: identify the behavior of subpopulations of GLT-1, if they exist, and localize single nanoparticles molecules with sub-wavelength precision. The use of nanometer-sized particle complexes make even possible to track GLT-1 within confined cellular compartments, such as the glutamate synapse environment. The precision by which a surface GLT-1 can be tracked and placed in a given cellular compartment comes from the pointing accuracy of the single nanoparticle, which acts as a single emission point. In our imaging device, the pointing accuracy is in the range of 20–30 nm. Thus, although we did not perform super-resolution microscopy, the single nanoparticle tracking allowed us to reconstitute high-precision X-Y trajectories with a high image acquisition rate (20 Hz)[22].

Single nanoparticle tracking of GLT-1^{flag}–transfected astrocytes in mixed hippocampal cultures revealed that individual GLT-1 transporters were highly mobile on the surface of astrocytes (**Fig. 1b–d**). The mean square displacement (area explored over time, MSD) of GLT-1 transporters showed a negative curvature characteristic of confined behavior (**Fig. 1e**), suggesting the presence of regulatory mechanisms[22]. Under basal conditions, GLT-1 had a median instantaneous diffusion coefficient of 0.23 μm^2 s^{-1} (interquartile range (IQR) ± 0.12–0.36 μm^2 s^{-1}; **Fig. 1c**) and an immobile fraction of only 6% (diffusion coefficient < 0.005 μm^2 s^{-1}; **Fig. 1c**), showing highly dynamic properties compared with those reported for neuronal[19,23], astrocytic[20] and microglial[21] receptors (immobile fractions comprised between 25 and 80%). Notably, the majority of QD-tagged GLT-1 was located at the surface during imaging sessions, and not in an internalized pool (**Supplementary Fig. 1b,c**). To determine whether these parameters are specific for GLT-1 or are common for all types of transmembrane transporters, we characterized the surface diffusion of another transporter, the dopamine transporter (DAT; **Supplementary Fig. 1d**), which has been reported to be expressed on astrocytes, although the functional relevance of this expression remains unresolved[24]. We observed that DAT transporters diffused substantially slower and in a more confined manner than GLT-1 (**Supplementary Fig. 1e–g**), demonstrating that GLT-1 and DAT diffusion properties are different, potentially as a result of the presence of different interactions or directly by the presence or absence of their substrates (glutamate and dopamine). Together, these data indicate that surface GLT-1 exhibits markedly high and somehow regulated dynamics on hippocampal astrocytes.

Activity-dependent regulation of GLT-1 surface diffusion

Given that neuronal activity affects expression levels of GLT-1 on astrocytes[25,26], we investigated the possibility that GLT-1 membrane mobility is also activity dependent. Monitoring GLT-1 surface trafficking in neuron-free cultures revealed that GLT-1 was almost immobile, with a diffusion coefficient 84% slower than in mixed cultures (**Fig. 1f,g**). Similarly, blocking action potential firing in mixed cultures using the voltage-gated sodium channel blocker tetrodotoxin (TTX, 1 μM) also reduced GLT-1 diffusion (42% decrease; **Fig. 1f,g**), indicating that neuronal activity is an important regulator of GLT-1 surface trafficking. We next assessed whether the transport activity of GLT-1 affected its surface mobility. In the presence of TBOA (30 μM), a specific non-transportable antagonist of glutamate transporters, GLT-1 diffusion was reduced by 36% (**Fig. 1g,h**), suggesting that transport activity does indeed contribute to GLT-1 membrane diffusion. Moreover, exposing mixed cultures to glutamate (100 μM), the substrate of GLT-1, induced an immediate 36% increase in GLT-1 diffusion (**Fig. 1f,g**).

To elucidate whether this effect is a result of a direct action of glutamate on the transporter or is mediated through the activation of glutamate receptors, we repeated this experiment in the presence of antagonists inhibiting NMDA (AP5, 10 μM), AMPA (NBQX, 10 μM) and metabotropic glutamate receptors (MCPG, 500 μM). This cocktail alone reduced GLT-1 surface diffusion by 17% (**Fig. 1f,g**), further implicating neuronal and possibly astrocytic activity, through receptor activation, in the regulation of GLT-1 diffusion. Notably, in these conditions, glutamate still facilitated the membrane diffusion of GLT-1, but to a lower extent than glutamate alone (13% versus 36% with glutamate alone; **Fig. 1g**). These results confirm that neuronal, glial and the transport activity of GLT-1 contribute to the regulation of this transporter's surface mobility.

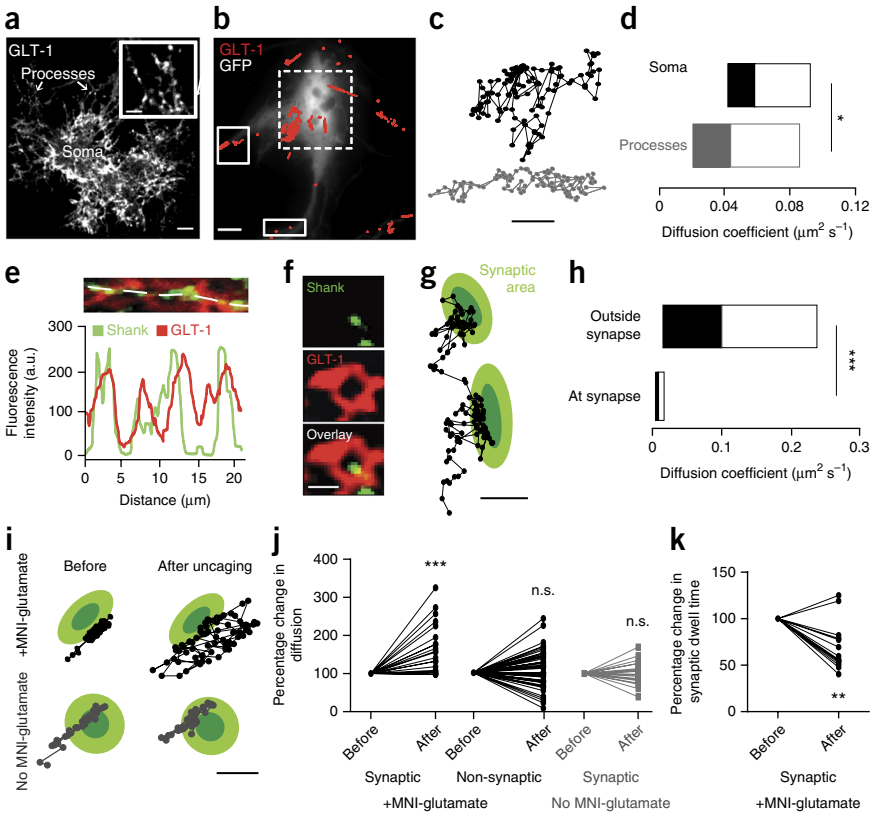

Figure 2 GLT-1 diffusion is compartmentalized on the surface of astrocytes. (**a**) Single-plane confocal microscopy image of an astrocyte stained for GLT-1^{flag}. Scale bar represents 10 μm. Inset, magnification of astrocyte processes showing GLT-1 clusters. Scale bar represents 2 μm. (**b**) GLT-1^{flag}–QD trajectories on an eGFP-expressing astrocyte. Broken line box, somatic trajectories; continuous line boxes, trajectories on processes. Scale bar represents 5 μm. (**c**) Representative GLT-1^{flag} trajectories from the soma and processes. Scale bar represents 0.5 μm. (**d**) Instantaneous GLT-1 diffusion coefficient distribution on the soma and processes (median ± IQR; soma: 0.059 ± 0.042–0.091 μm^2 s^{-1}, n = 1, 601 trajectories; processes: 0.043 ± 0.022–0.083 μm^2 s^{-1}, n = 416 trajectories; $^*P$ = 0.04). (**e**,**f**) Single-plane confocal microscopy images of a hippocampal culture stained for surface GLT-1^{flag} and the synaptic protein Shank (green). Scale bar represents 1 μm. Graph, line scan profile showing the correlation between GLT-1^{flag} and Shank staining. (**g**) Representative trajectory of a single GLT-1^{flag} entering a synapse, exiting and reaching another synaptic area. Scale bar represents 0.5 μm. (**h**) Instantaneous GLT-1 diffusion coefficient distribution at and outside synapses (at synapse: 0.0013 ± 0.000014–0.0046 × 10^{-3} μm^2 s^{-1}, n = 61 trajectories; outside synapse: 0.089 ± 0.008–0.22 μm^2 s^{-1}, n = 444 trajectories; $^{***}P < 0.001$). (**i**) Representative trajectories of a single GLT-1^{flag} at a synapse, before and after uncaging in the presence (top) or absence (bottom) of MNI-caged glutamate. Scale bar represents 0.32 μm. (**j**) Percentage change in GLT-1 surface diffusion before and after uncaging laser at the synapse (n = 21 trajectories, $^{***}P < 0.001$), at nonsynaptic sites (n = 53 trajectories, P = 0.27, n.s.) and in the absence of MNI-caged L-glutamate (n = 22 trajectories, P = 0.68, n.s.). (**k**) Significant decrease in synaptic dwell time for GLT-1 transporters after uncaging (n = 14 trajectories, $^{**}P$ = 0.0013).

Diffusion of GLT-1 varies according to its surface location

Because astrocytes display complex cellular arborization and specialized domains, we investigated whether GLT-1 surface trafficking differs according to its cell surface location. Immunostaining confirmed that GLT-1 can be found all over the soma and processes, as previously reported[27] (**Fig. 2a**). Live imaging of surface diffusion revealed that GLT-1 diffusion was slower in the processes (**Fig. 2b–d**). We hypothesized that this reduction may result from the presence of synaptic contacts at astrocytic processes, a location at which GLT-1 are supposedly anchored. Indeed, immunostaining of fixed hippocampal mixed cultures revealed a strong positive correlation between GLT-1 and synaptic markers (**Fig. 2e**). In several cases, a ring of GLT-1 was observed surrounding clusters of a postsynaptic scaffold protein, Shank (**Fig. 2f**). To further tackle this question, we assessed diffusion parameters in the vicinity of excitatory synapses labeled by electroporation of Homer1c-dsRed, another postsynaptic scaffold protein. Notably, the surface diffusion of GLT-1 transporters slowed down markedly whenever entering a synaptic site and recovered after exiting the synapse (**Fig. 2g,h**), indicating that GLT-1 transporters diffuse in and out of glutamatergic synapses in which they are stabilized.

As demonstrated above, glutamate application increases the surface diffusion of GLT-1 transporters. Together with the finding that GLT-1 transporters are stabilized at synaptic sites, one may suggest that glutamate release from the presynaptic terminal 'unleashes' GLT-1 transporters. To directly test this possibility, we determined the effect of glutamate release on GLT-1 diffusion at or near synapses by mimicking synaptic release using caged glutamate. Following glutamate

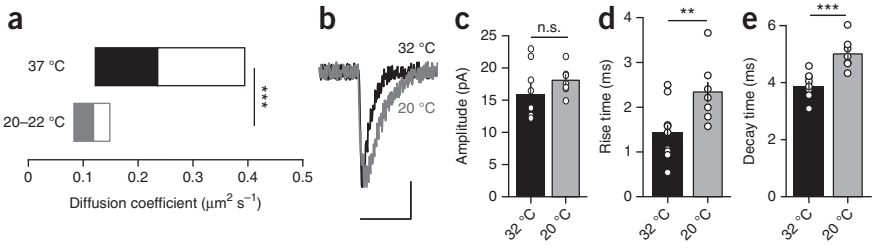

Figure 3 Effect of temperature on GLT-1 diffusion and sEPSC kinetics. (**a**) GLT-1 diffusion was significantly slower at 20–22 °C than at 37 °C (median ± IQR; 37 °C: 0.23 ± 0.12–0.36 μm^2 s^{-1}, n = 720 trajectories; 20–22 °C: 0.12 ± 0.08–0.15 μm^2 s^{-1}, n = 322 trajectories; $^{***}P < 0.001$). (**b**) Superimposition of sEPSC recorded at 32 °C (black) and 20 °C (gray) conditions. Scale bars represent 20 pA and 10 ms. (**c**) No difference in sEPSC amplitude between 20 °C and 32 °C (mean ± s.e.m.; 32 °C: 15.9 ± 1.72 pA, n = 9 neurons; 20 °C: 18 ± 2.17 pA, n = 7 neurons; P = 0.13, n.s.). (**d**,**e**) Both rise time (mean ± s.e.m.; 32 °C: 1.5 ± 0.17 ms, n = 9 neurons; 20 °C: 2.3 ± 0.21 ms, n = 7 neurons; $^{**}P$ = 0.003) and decay (mean ± s.e.m.; 32 °C: 3.7 ± 0.14 ms, n = 9 neurons; 20 °C: 5.0 ± 0.21 ms, n = 7 neurons; $^{***}P < 0.001$) were increased at 20 °C compared with 32 °C.

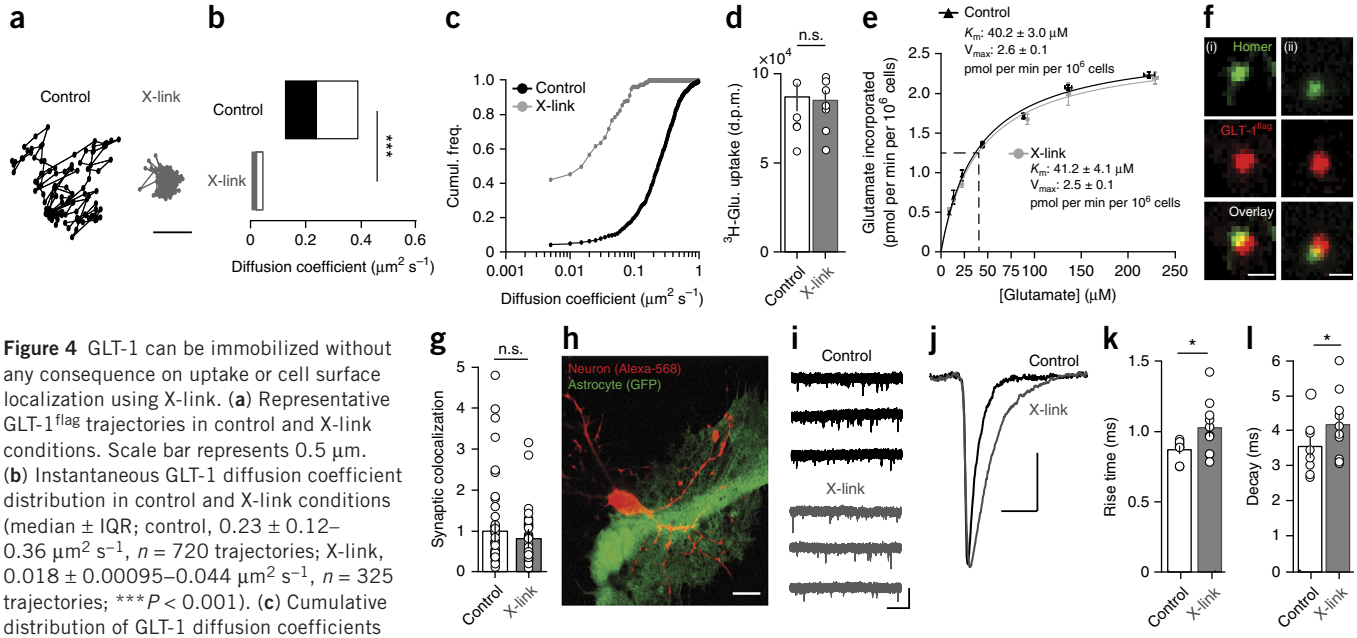

Figure 4 GLT-1 can be immobilized without any consequence on uptake or cell surface localization using X-link. (**a**) Representative GLT-1^{flag} trajectories in control and X-link conditions. Scale bar represents 0.5 μm. (**b**) Instantaneous GLT-1 diffusion coefficient distribution in control and X-link conditions (median ± IQR; control, 0.23 ± 0.12–0.36 μm^2 s^{-1}, n = 720 trajectories; X-link, 0.018 ± 0.00095–0.044 μm^2 s^{-1}, n = 325 trajectories; ***P < 0.001). (**c**) Cumulative distribution of GLT-1 diffusion coefficients in control and X-link conditions. (**d**) GLT-1^{flag} retained full uptake capacity in X-link condition (mean ± s.e.m.; control: 87,173 ± 7,562 d.p.m., n = 8 coverslips; X-link: 85,211 ± 5,719 d.p.m.; n = 8 coverslips; P = 0.8, n.s.). (**e**) Saturation analysis of L-glutamate uptake into GLT-1–transfected COS-7 cells used to calculate the affinity of GLT-1 for glutamate, in control and X-link conditions. Dashed line indicates K_m for both control and X-link, which overlap on graph (control: 40.2 ± 3.0 μM, n = 7; X-link: 41.2 ± 4.1 μM, n = 7 cell cultures; P = 0.9, n.s.). V_{max} is reported on the graph (control: 2.6 ± 0.1 pmol per min per 10^6 cells, n = 7; X-link: 2.5 ± 0.1 pmol per min per 10^6 cells, n = 7; P = 0.9, n.s.). Data are presented as mean ± s.e.m. (**f**) Maximum projection of confocal images in Z, showing GLT-1^{flag} expression around Homer1c-dsRed–labeled synapses (green) in control (i) and X-link (ii) conditions. Scale bar represents 1 μm. (**g**) Normalized colocalization levels between GLT-1^{flag} and the synaptic marker Homer-1 (mean ± s.e.m.; control, n = 46 individual synapses; X-link, n = 31; P = 0.5484, n.s.). (**h**) Example of Alexa-568–filled neuron (red) recorded in whole-cell patch-clamp, covered by a GFP/GLT-1^{flag}–transfected astrocyte (green). Scale bar represents 3 μm. (**i**) Representative sEPSC recorded from hippocampal neurons in control and X-link conditions. Scale bars represent 50 pA and 500 ms. (**j**) Superimposition of sEPSC recorded in control (black) and X-link (gray) conditions. Scale bars represent 10 pA and 10 ms. (**k**,**l**) X-link of GLT-1 increased the rise (mean ± s.e.m.; control: 0.87 ± 0.03 ms, n = 8 neurons; X-link: 1.0 ± 0.06 ms, n = 10 neurons; *P = 0.025) and decay time (mean ± s.e.m.; control: 3.5 ± 0.2 ms, n = 8 neurons; X-link: 4.2 ± 0.2 ms, n = 10 neurons; *P = 0.04) of AMPAR sEPSCs.

uncaging close to synaptic sites, we observed a rapid increase in GLT-1 diffusion (56% increase; **Fig. 2i,j**), which was not the case for uncaging at nonsynaptic sites nor in the absence of MNI-glutamate (nonsynaptic, 0% change; no MNI-glutamate, 2% increase; **Fig. 2i,j**). Notably, glutamate uncaging at synapses resulted in the displacement of GLT-1 away from the synapse, with synaptic dwell time strongly reduced following glutamate uncaging (31% decrease after uncaging; **Fig. 2k**). Together, these findings confirm that GLT-1 is indeed anchored at synapses and can be untethered following exposure to glutamate.

Surface diffusion of GLT-1 shapes synaptic transmission

On the basis of this dynamic surface mobility, one may propose that lateral diffusion allows transporters to switch in and out synaptic areas, enabling glutamate-bound GLT-1 to leave synaptic sites and naive unbound GLT-1 to reach these confined spaces. This hypothesis is supported by the fact that if transporters were static, there would need to be equal or more GLT-1 than glutamate molecules released at the synapse based on their cycling time[4,6,7]. Initially, we tested this hypothesis by manipulating temperature, as it has been demonstrated

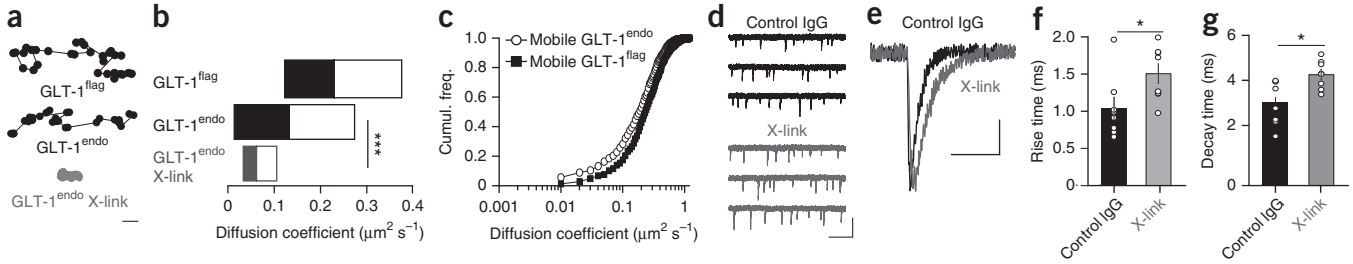

Figure 5 Surface diffusion of GLT-1 confers synaptic glutamate homeostasis on fast timescale. (**a**) Representative trajectories of GLT-1^{flag} in control conditions and GLT-1^{endo} in control and X-link conditions. Scale bar represents 0.5 μm. (**b**) Instantaneous diffusion coefficients of GLT-1^{flag} (median ± IQR; diffusion coefficient: 0.23 ± 0.12–0.36 μm^2 s^{-1}, n = 720 trajectories) compared with the GLT-1^{endo} in control (median ± IQR; diffusion coefficient: 0.13 ± 0.014–0.273 μm^2 s^{-1}, n = 668 trajectories) and X-link (median ± IQR; diffusion coefficient: 0.06 ± 0.033–0.105 μm^2 s^{-1}, n = 326 trajectories, ***P < 0.001) conditions. (**c**) Cumulative distribution of the mobile fraction of GLT-1^{flag} and GLT-1^{endo} in control conditions. (**d**) Representative sEPSC recorded from hippocampal neurons *in vitro* in control and X-link conditions. Scale bars represent 50 pA and 200 ms. (**e**) Superimposition of sEPSC recorded in control (black) and X-link (gray) conditions. Scale bars represent 20 pA and 10 ms. (**f**,**g**) X-link of GLT-1^{endo} increased both rise (mean ± s.e.m.; control: 1.0 ± 0.15 ms, n = 8 neurons; X-link: 1.5 ± 0.13 ms, n = 8 neurons; *P = 0.038) and decay time (mean ± s.e.m.; control: 3.3 ± 0.3 ms, n = 8 neurons; X-link: 4.4 ± 0.2 ms, n = 8 neurons; *P = 0.028) of sEPSCs.

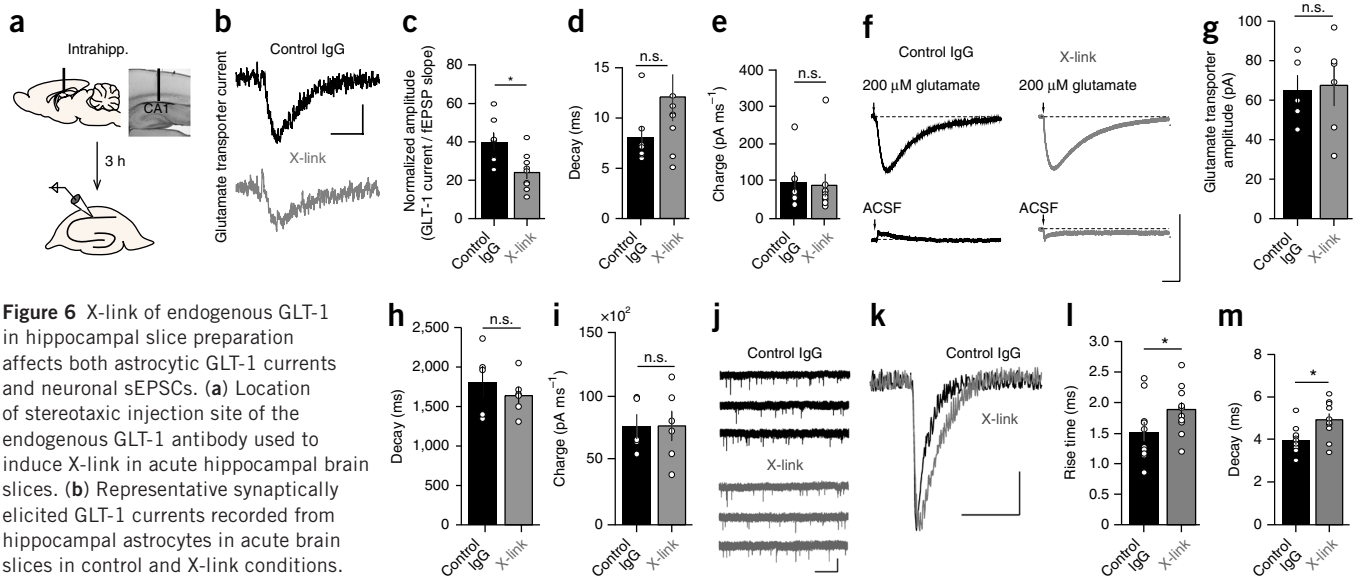

Figure 6 X-link of endogenous GLT-1 in hippocampal slice preparation affects both astrocytic GLT-1 currents and neuronal sEPSCs. (**a**) Location of stereotaxic injection site of the endogenous GLT-1 antibody used to induce X-link in acute hippocampal brain slices. (**b**) Representative synaptically elicited GLT-1 currents recorded from hippocampal astrocytes in acute brain slices in control and X-link conditions. Scale bars represent 5 pA and 10 ms. (**c**) Normalized amplitude of GLT-1 transporter currents (GLT-1 current / fEPSP slope; mean ± s.e.m.; control: 39.8 ± 4.7, $n = 7$ astrocytes; X-link: 23.9 ± 3.2, $n = 9$; $^*P = 0.023$). (**d**) Decay time of GLT-1 transporter currents (mean ± s.e.m.; control: 8.1 ± 1.1 ms, $n = 7$ astrocytes; X-link: 12.1 ± 2.3 ms, $n = 9$; $P = 0.18$, n.s.). (**e**) Charge transfer of GLT-1 transporter currents (mean ± s.e.m.; control: 95.4 ± 26.6 pA ms^{-1}, $n = 7$ astrocytes; X-link: 91.2 ± 29.2 pA ms^{-1}, $n = 9$; $P = 0.74$, n.s.). (**f**) Representative glutamate transport currents recorded from hippocampal astrocytes in presence of a cocktail of ionotropic and metabotropic receptor antagonists (Online Methods) following glutamate puff application in acute brain slices in control and X-link conditions. Scale bars represent 100 pA and 500 ms. Note that the glutamate-induced transport current was potentiated by the glutamate transporter antagonist TBOA, consistent with former observations[5]. (**g**) Amplitude of glutamate puff–elicited GLT-1 transporter currents (mean ± s.e.m.; control: 64.9 ± 7.5, $n = 5$ astrocytes; X-link: 67.6 ± 9.6, $n = 6$; $P = 0.87$, n.s.). (**h**) Decay time of glutamate puff–elicited GLT-1 transporter current (mean ± s.e.m.; control: 1,808 ± 191.9 ms, $n = 5$ astrocytes; X-link: 1,637 ± 99.9 ms, $n = 6$; $P = 0.65$, n.s.). (**i**) Charge transfer of glutamate puff–elicited GLT-1 transporter currents (mean ± s.e.m.; control: 76,480 ± 9,121 pA ms^{-1}, $n = 5$ astrocytes; X-link: 77,025 ± 11,169 pA ms^{-1}, $n = 6$; $P = 0.87$, n.s.). (**j**) Representative sEPSC recorded from hippocampal neurons in acute brain slices in control and X-link conditions. Scale bars represent 50 pA and 500 ms. (**k**) Superimposition of sEPSC recorded in control (black) and X-link (gray) conditions. Scale bars represent 20 pA and 10 ms. (**l**,**m**) X-link of GLT-1 increased the rise (mean ± s.e.m.; control: 1.53 ± 0.07 ms, $n = 10$ neurons; X-link: 1.89 ± 0.13 ms, $n = 10$; $^*P = 0.024$) and decay time (mean ± s.e.m.; control: 4.0 ± 0.2 ms, $n = 10$ neurons; X-link: 4.9 ± 0.3 ms, $n = 10$; $^*P = 0.014$) of sEPSCs.

that surface diffusion of receptors, a Brownian process, is temperature dependent[28]. Furthermore, temperature can have a great effect on GLT-1 function, with cycling time substantially increased at physiological temperature compared with 20–22 °C. As expected, QD imaging of GLT-1 at both 37 °C and 20–22 °C revealed that the speed of diffusion of the transporter was decreased at lower temperatures (**Fig. 3a**). Continuing on this line of enquiry, we recorded spontaneous excitatory postsynaptic currents (sEPSCs) in hippocampal neurons in acute brain slices at 32 °C and 20 °C and observed that decreasing temperature affected the kinetics of sEPSCs, increasing both rise time and decay without affecting the amplitude of individual events (**Fig. 3b–e**). Although the change in EPSC kinetics is very likely related, at least partially, to the modified cycling time of the transporter, it could also reflect the altered GLT-1 membrane diffusion occurring under these conditions.

Next, we directly tested this hypothesis in neuron-glia networks. We adapted a cross-linking (X-link) strategy to immobilize GLT-1 at the cell surface using a high concentration of primary antibodies (200 µg ml^{-1}; **Fig. 4a**), as previously described[19,29,30]. X-link consistently reduced the mobility (**Fig. 4b**) and increased the immobile fraction of GLT-1 by 36% (**Fig. 4c**). The X-link procedure did not affect the transport activity of GLT-1, as attested by glutamate uptake measurements in GLT-1^{flag}–transfected COS-7 cells (**Fig. 4d**), did not alter the affinity of GLT-1 for glutamate, with no difference observed in K_m and V_{max} (**Fig. 4e**), and did not hinder the access of GLT-1 to the synapse, as revealed by immunostaining in mixed hippocampal cultures (**Fig. 4f,g**) between control and X-link conditions. Certain that X-link of GLT-1 only affects the diffusion of the transporter, we then evaluated the functional consequences of GLT-1 X-link on excitatory neurotransmission *in vitro* by recording spontaneous excitatory postsynaptic currents (sEPSC) from neurons closely associated with GLT-1^{flag}–transfected astrocytes (**Fig. 4h,i**) and exposed to either control (nonspecific) antibodies or specific antibodies inducing the GLT-1 X-link (**Fig. 4a**). Although sEPSC amplitude (control: 27.5 ± 2.1 pA, $n = 8$ neurons; X-link: 25.7 ± 4.2 pA, $n = 10$ neurons; $P = 0.37$) and frequency (control: 6.8 ± 2.5 Hz, $n = 8$ neurons; X-link 5.9 ± 1.6 Hz, $n = 10$ neurons; $P = 0.38$) were unaltered (**Table 1**), both the rise time and decay were increased in X-link conditions (118% and 119% of control, respectively; **Fig. 4j–l** and **Table 1**).

Although GLT-1^{flag} provides high specificity in tracking glutamate transporters *in vitro*, it does not allow us to assess the physiological role of GLT-1diffusion in more intact brain preparations, where the astrocytic coverage of synapses may differ. To overcome this limitation, we performed a similar series of experiments using an antibody to an extracellular epitope of endogenous GLT-1 (GLT-1^{endo}). We first characterized the diffusion of GLT-1^{endo} *in vitro* and observed that the diffusion coefficient was slower and confinement was higher than GLT-1^{flag} (**Fig. 5a,b** and **Supplementary Fig. 2a**). This finding could be explained by the fact that this antibody recognizes all isoforms of GLT-1 that differ only in the intracellular N- and C termini. Indeed, a direct comparison of the mobile fraction of GLT-1^{flag} and GLT-1^{endo} revealed a high similarity regarding the diffusion properties of mobile transporters (**Fig. 5c**). As for GLT-1^{flag}, we were able to induce a X-link of GLT-1^{endo} using a high concentration of primary antibodies (**Fig. 5a,b**).

Table 1 Electrophysiology results

	Amplitude (pA)	Frequency (Hz)	Rise time (ms)	Decay (ms)	*n* (cells)
Mixed hippocampal culture					
GLT-1^{flag}					
Control	27.5 ± 2.1	6.8 ± 2.5	0.87 ± 0.03	3.5 ± 0.2	8
X-link	25.7 ± 4.2	5.9 ± 1.6	1.0 ± 0.06*	4.2 ± 0.2*	10
GLT-1^{endo}					
Control	33.2 ± 4.2	7.5 ± 2.9	1.0 ± 0.15	3.3 ± 0.3	8
X-link	27.3 ± 4.4	6.2 ± 2.4	1.5 ± 0.13*	4.4 ± 0.2*	8
Acute brain slice					
Neuronal recordings (sEPSC)					
Control	21.0 ± 1.4	0.84 ± 0.12	1.53 ± 0.07	4.0 ± 0.2	10
X-link	25.8 ± 2.8	0.58 ± 0.13	1.89 ± 0.13*	4.9 ± 0.3*	10
Synaptically activated glutamate transporter currents					
	Normalized (GLT-1 current/fEPSP slope; a.u.)				
Control	39.8 ± 4.7	N/A	3.03 ± 0.31	8.1 ± 1.1	7
X-link	23.9 ± 3.2*	N/A	3.03 ± 0.66	12.1 ± 2.3	9
Puff-elicited glutamate transporter currents					
Control	64.9 ± 7.5	N/A	N/A	1808 ± 191.9	5
X-link	67.6 ± 9.6	N/A	N/A	1637 ± 99.9	6

Data are presented as mean ± s.e.m.; *$P < 0.05$.

Notably, we found no difference in the total glutamate uptake in mixed hippocampal cultures subjected to either the antibody to Flag or that to endogenous GLT-1 at control and X-link concentrations (**Supplementary Fig. 2b**), confirming that the X-link procedure by itself does not affect the transport function of GLT-1.

We then examined the functional role of surface diffusion of GLT-1^{endo} on neuronal activity by recording sEPSCs in the presence or absence of GLT-1^{endo} X-link *in vitro*. Exactly as observed in GLT-1^{flag} conditions, induction of GLT-1^{endo} X-link had no effect on the amplitude (control: 33.2 ± 4.2 pA, $n = 8$ neurons; X-link: 27.3 ± 4.4 pA, $n = 8$ neurons; $P = 0.065$) or the frequency (control: 7.5 ± 2.9 Hz, $n = 8$ neurons; X-link 6.2 ± 2.4 Hz, $n = 8$ neurons; $P = 0.83$) of individual synaptic events (**Fig. 5d**,**e** and **Table 1**), but the X-link modified sEPSC kinetics, increasing both rise (**Fig. 5f** and **Table 1**) and decay (**Fig. 5g** and **Table 1**) times. It could be noted that the GLT-1^{endo} X-link condition increased the rise and decay times by approximately 44 and 33%, whereas the increases were 18 and 19%, respectively, in GLT-1^{flag} condition, as expected by the widespread distribution of the endogenous GLT-1. These results validate our previous findings and rule out the possibility that the effects that we observed using GLT-1^{flag} were a result of overexpression of the transporter. To further address this question, we carried out immunostaining to quantify the level of total GLT-1 expression in GLT-1^{flag}–transfected and non-transfected astrocytes in mixed cultures. Although expression levels were highly variable between cells, we did not observe a difference in the total levels of GLT-1 expression in astrocytes transfected with GLT-1^{flag} compared to non-transfected astrocytes (**Supplementary Fig. 3a**,**b**).

Having validated a procedure to immobilize endogenous GLT-1, we next investigated whether interfering with GLT-1 diffusion in an *ex vivo* brain preparation, that is, acute hippocampal slices, could also affect excitatory neurotransmission. X-link of GLT-1^{endo} in acute slices was achieved by *in vivo* stereotaxic injection of antibody to GLT-1 into the CA1 area of the hippocampus of anesthetized rats. Animals were allowed to recover for 1 h before death and slice preparation (**Fig. 6a**). Given that we hypothesize that GLT-1 membrane trafficking at synaptic sites is important to maximize the clearance of synaptically released glutamate, we first recorded synaptic activity-elicited glutamate transporter currents from astrocytes in our hippocampal slice preparation. X-link of GLT-1 resulted in a decrease in the amplitude of synaptically activated transporter currents (**Fig. 6b**,**c** and **Table 1**), whereas no change was observed in the decay, although a tendency toward an increase was noticed in slices from X-link–injected animals (**Fig. 6d** and **Table 1**). Notably, the charge transfer of these currents was unchanged between control and X-link conditions (**Fig. 6e**), supporting the conclusion that, although GLT-1 immobilization may delay the uptake of synaptically released glutamate, the total amount of glutamate taken up is similar under control and X-link conditions. Finally, to rule out an effect of *in vivo* X-link on the transport activity of GLT-1 itself, we next recorded astrocytic GLT-1 transporter currents in response to puffs of glutamate (**Fig. 6f**) that activate a large fraction of astrocytic transporters and should allow us to observe any fine changes in glutamate transporter current. No modifications were detected either in amplitude, decay or charge transfer between control and X-link conditions following 40-ms puffs (10 psi) of 200 µM glutamate (**Fig. 6f–i** and **Table 1**), demonstrating that X-link does not affect the global glutamate uptake ability of astrocytic GLT-1 *ex vivo*. Altogether, our data agree with the proposition that cross-linking does not alter the transport function of GLT-1 (K_m and V_{max}, synaptically activated glutamate transporter currents, puff-elicited glutamate transporter currents), but it does reduce the supply of unbound GLT-1 needed to diffuse into the synaptic cleft and effectively remove glutamate from this confined space without inducing undesired effects.

We then turned our attention back to the effect of GLT-1 X-link on neuronal activity, this time in the hippocampal slice preparation. X-link was achieved in the same manner as when recording GLT-1 currents from astrocytes, that is, *in vivo* stereotaxic injection. As in culture, no change was observed in amplitude (control: 21.0 ± 1.4 pA, $n = 10$ neurons; X-link: 25.8 ± 2.8 pA, $n = 10$; $P = 0.14$) or frequency (control: 0.84 ± 0.12 Hz, $n = 10$ neurons; X-link 0.58 ± 0.13 Hz, $n = 10$; $P = 0.5$) of sEPSCs between control and X-link conditions in the acute brain slice (**Fig. 6j**,**k** and **Table 1**). Notably, X-link elicited an increase in rise time and decay of sEPSCs (**Fig. 6k–m** and **Table 1**) equivalent to those observed *in vitro*. These findings are consistent with a reduced glutamate buffering function, as similar changes have been observed when glutamate uptake is altered pharmacologically[14,15,31]. Collectively, these data demonstrate that surface diffusion allows GLT-1 to rapidly move between synaptic and nonsynaptic sites, thereby ensuring glutamate clearance and shaping excitatory postsynaptic currents (**Supplementary Fig. 4**).

DISCUSSION

We used a combination of high-resolution live imaging and electrophysiological approaches to assess the role of GLT-1 diffusion at the surface of astrocytes in the regulation of glutamate clearance from synapses. We found that GLT-1 transporters are not static, but are instead highly mobile at the surface of astrocytes, and that this surface diffusion is dependent on both neuronal and glial cell activities. Impairment of GLT-1 transporter lateral diffusion through cross-linking both *in vitro* and *ex vivo* in acute hippocampal brain slices has a direct effect on the kinetics of excitatory postsynaptic currents, consistent with an altered glutamate clearance from

the synapse. These data reinforce the concept that astrocytes are actively involved in shaping excitatory neurotransmission, and place surface diffusion of glutamate transporters as a new pivotal feature of the tripartite synapse.

The importance of astrocytic transporters for glutamate clearance has been widely acknowledged[9,32,33], with undeniable evidence suggesting that GLT-1 is vital for removing glutamate from the extracellular space[34]. Research on the glutamate uptake mechanism(s) has been very fruitful, demonstrating the complexity in structure[35], kinetics[4,5] and physiological role[7,16] of this family of transporters. It has been estimated that each individual glutamatergic vesicle carries approximately 4,000 glutamate molecules[2]. On the basis of this evidence, and the techniques available at the time, it was suggested that equal numbers of transporters and glutamate molecules are required for these transporters to efficiently clear this neurotransmitter[7]. Support for this hypothesis was provided using immunoblots from lysed brain tissue, from which the concentration of GLT-1 was calculated to be on the order of 8,500 proteins per μm^2 of astrocyte membrane in the hippocampus[6], making GLT-1 one of the highest expressed proteins in the brain (1% of total brain protein). However, high expression alone cannot account for the dynamic regulation of synaptic transmission repeatedly observed in the literature. Recent evidence has suggested that the precise location of astrocytic processes expressing glutamate transporters can directly affect glutamate uptake[36–39]. These studies have demonstrated that GLT-1–containing astrocytic processes are located approximately in a 400-nm-radius circle from the core synapse[38,39], with further evidence suggesting that it is the close apposition of GLT-1–containing astrocytic processes to the synaptic area that permits astrocytes to control glutamatergic synaptic transmission[37]. Here, we add another layer of complexity to this glutamate uptake system and shed new light on glutamate uptake at synaptic sites.

We found that surface trafficking of astroglial GLT-1 features several characteristics that make it unique: the diffusion coefficient of GLT-1 was among the highest reported, the fraction of immobile transporters was one of the lowest reported in the literature and pharmacological manipulations produced rapid bidirectional effects on GLT-1 diffusion, reflecting an activity-dependent regulation of transporter dynamics. The sensitivity of GLT-1 to neuronal and its own functional activity was notable and highlights the importance of this transporter in regulating glutamate homeostasis in the extracellular space. GLT-1 not only responded to high-activity conditions by increasing its surface diffusion, but also reacted to low-activity by reducing surface diffusion. Further observations revealed that GLT-1 surface diffusion was strongly reduced in the vicinity of synapses. This indicates the presence of a regulatory mechanism that has thus far remained elusive. On the basis of our most recent understanding of receptor dynamics at synapses[40], such results could be explained by the presence of scaffolding and anchoring proteins and/or of a hindered molecular environment. This is consistent with the existence of a specialized astrocytic compartment in the vicinity of synapses in which GLT-1 transporters, and possibly other proteins, could interact to serve synaptic functions.

The observation that GLT-1 diffusion is reduced in the vicinity of synapses strengthens our hypothesis that surface diffusion of GLT-1 has a role in removing glutamate from the synapse. We propose that synaptically localized GLT-1 binds glutamate, increasing GLT-1 diffusion, which then moves away from the synapse, possibly allowing naive (not bound) extrasynaptic transporters to diffuse into the synaptic cleft. This hypothesis was further strengthened by experiments mimicking glutamate release through glutamate uncaging, in which we found that the presence of glutamate at the synapse reversed this synaptic stabilization, increasing GLT-1 surface diffusion and displacement away from the synaptic area.

Surface diffusion of glutamate receptors on neurons has been recently shown to contribute to the regulation of glutamatergic synaptic transmission[19,30]. By artificially immobilizing GLT-1 while fully preserving its transport function, we found both *in vitro* and in acute hippocampal slices that surface diffusion of glutamate transporters on astrocytes shaped sEPSC kinetics, fueling the hypothesis that it could also contribute to this regulation by controlling the concentration of glutamate at the synapse. Furthermore, synaptically evoked glutamate transporter currents recorded in astrocytes were substantially reduced in X-link conditions, indicating that, over time, surface diffusion of GLT-1 influences the size of transporter currents at synaptic sites. It is also consistent with the assumption that immobilizing GLT-1 through X-link affects glutamate clearance in the cleft, possibly by preventing naive transporters from entering the synaptic area and clearing glutamate.

Several studies have consistently found that transporters have an active role in controlling the time course of synaptic glutamate[14–16]. However, these studies reported the consequences of pharmacological blockade of transporters, whereas we merely immobilized GLT-1 surface diffusion without affecting their function. A general consensus is that glutamate transporters have a vital role in controlling the time course of glutamate in the synaptic cleft, with the strongest findings occurring at cerebellar synapses[14,41]. In the cerebellum, Bergmann glia (specialized astrocytes) are believed to completely ensheath Purkinje cell synapses[42], markedly limiting the implication of diffusion of glutamate in the clearance of this neurotransmitter from the cleft. At hippocampal synapses, some studies have stated that transporters are not important in controlling the time course of synaptic glutamate as a result of the supposed low level of coverage of synapses by astrocytes[42] and observation of heterosynaptic glutamate spillover[43]. Since then, further work has shown that the role of transporters at hippocampal synapses has been underestimated[17,18]. These studies highlighted the importance of experimenting at near-physiological temperatures, as glutamate uptake, diffusion of glutamate and glutamate receptor activation are temperature-dependent processes[4,16–18]. Furthermore, surface diffusion of proteins, including receptors[28] and transporters, is also a temperature-dependent process.

Trafficking of neurotransmitter receptors at the surface of neurons is important for controlling receptor distribution and synaptic signaling in physiological as well as pathological processes[44,45]. Consequently, it is not far-fetched to consider the possibility of a failure in the regulatory mechanisms controlling glutamate transporter surface diffusion under certain pathological conditions. It has previously been demonstrated that disruption of this vital neurotransmitter clearance mechanism contributes to many neurodegenerative diseases, including amyotrophic lateral sclerosis, epilepsy, Alzheimer's, Huntington's and Parkinson's disease[46–50]. Thus, in addition to improving our understanding of the contribution of transporters in controlling glutamate at the synapse, this unexpected mechanism opens new avenues of research for neurological and psychiatric disorders involving a dysfunction of glutamate transport.

METHODS

Methods and any associated references are available in the online version of the paper.

Note: Any Supplementary Information and Source Data files are available in the online version of the paper.

ACKNOWLEDGMENTS

We thank M. Rattray (University of Bradford) for the generous gift of GLT-1^{flag} construct, U. Gether (University of Copenhagen) for the generous gift of DAT^{flag} construct and M. Goillandeau (CNRS) who developed the software for the detection and analysis of synaptic events. We thank D. Bouchet (IINS CNRS), A. Ledantec (IINS CNRS) and N. Cassagno (INSERM) for cell cultures. We thank the Bordeaux Imaging Center, C. Poujol and D. Choquet for technical support. We thank our laboratory members for critical discussions. This work was supported by Centre National de la Recherche Scientifique, Institut National de la Santé et de la Recherche Médicale, Conseil Régional d'Aquitaine, Agence National de la Recherche, Fondation de la Recherche Medicale, LABEX BRAIN ANR-10-LABX-43, Marie Curie 'Edu-GLIA' (PITN-GA-2009-237, an Initial Training Network) and Marie Curie 'deepNMDAR' fellowship funded by the European Commission under the Seventh Framework Programme.

AUTHOR CONTRIBUTIONS

C.M.-R. carried out QD imaging, uncaging and immunostaining experiments and analysis. C.M.-R. and B.P. performed radiolabeled-glutamate uptake experiments and analysis. J.P.D. carried out electrophysiological experiments and analysis. J.A.V. and J.P.D. performed stereotaxic injections. A.P. recorded glutamate transporter currents. J.B. provided technical support. S.H.R.O. and L.G. directed the work. C.M.-R., J.P.D., L.G. and S.H.R.O. wrote the manuscript.

COMPETING FINANCIAL INTERESTS

The authors declare no competing financial interests.

1. Rothstein, J.D. *et al.* Localization of neuronal and glial glutamate transporters. *Neuron* **13**, 713–725 (1994).
2. Riveros, N., Fiedler, J., Lagos, N., Munoz, C. & Orrego, F. Glutamate in rat brain cortex synaptic vesicles: influence of the vesicle isolation procedure. *Brain Res.* **386**, 405–408 (1986).
3. Clements, J.D., Lester, R.A., Tong, G., Jahr, C.E. & Westbrook, G.L. The time course of glutamate in the synaptic cleft. *Science* **258**, 1498–1501 (1992).
4. Bergles, D.E. & Jahr, C.E. Glial contribution to glutamate uptake at Schaffer collateral-commissural synapses in the hippocampus. *J. Neurosci.* **18**, 7709–7716 (1998).
5. Wadiche, J.I., Arriza, J.L., Amara, S.G. & Kavanaugh, M.P. Kinetics of a human glutamate transporter. *Neuron* **14**, 1019–1027 (1995).
6. Lehre, K.P. & Danbolt, N.C. The number of glutamate transporter subtype molecules at glutamatergic synapses: chemical and stereological quantification in young adult rat brain. *J. Neurosci.* **18**, 8751–8757 (1998).
7. Diamond, J.S. & Jahr, C.E. Transporters buffer synaptically released glutamate on a submillisecond time scale. *J. Neurosci.* **17**, 4672–4687 (1997).
8. Arriza, J.L. *et al.* Functional comparisons of three glutamate transporter subtypes cloned from human motor cortex. *J. Neurosci.* **14**, 5559–5569 (1994).
9. Huang, Y.H. & Bergles, D.E. Glutamate transporters bring competition to the synapse. *Curr. Opin. Neurobiol.* **14**, 346–352 (2004).
10. Stenovec, M., Kreft, M., Grilc, S., Pangrsic, T. & Zorec, R. EAAT2 density at the astrocyte plasma membrane and Ca^{2+}-regulated exocytosis. *Mol. Membr. Biol.* **25**, 203–215 (2008).
11. Foran, E., Rosenblum, L., Bogush, A., Pasinelli, P. & Trotti, D. Sumoylation of the astroglial glutamate transporter EAAT2 governs its intracellular compartmentalization. *Glia* **62**, 1241–1253 (2014).
12. González, M.I. & Robinson, M.B. Neurotransmitter transporters: why dance with so many partners? *Curr. Opin. Pharmacol.* **4**, 30–35 (2004).
13. Kalandadze, A., Wu, Y. & Robinson, M.B. Protein kinase C activation decreases cell surface expression of the GLT-1 subtype of glutamate transporter. Requirement of a carboxyl-terminal domain and partial dependence on serine 486. *J. Biol. Chem.* **277**, 45741–45750 (2002).
14. Barbour, B., Keller, B.U., Llano, I. & Marty, A. Prolonged presence of glutamate during excitatory synaptic transmission to cerebellar Purkinje cells. *Neuron* **12**, 1331–1343 (1994).
15. Mennerick, S. & Zorumski, C.F. Glial contributions to excitatory neurotransmission in cultured hippocampal cells. *Nature* **368**, 59–62 (1994).
16. Tong, G. & Jahr, C.E. Block of glutamate transporters potentiates postsynaptic excitation. *Neuron* **13**, 1195–1203 (1994).
17. Asztely, F., Erdemli, G. & Kullmann, D.M. Extrasynaptic glutamate spillover in the hippocampus: dependence on temperature and the role of active glutamate uptake. *Neuron* **18**, 281–293 (1997).
18. Diamond, J.S. & Jahr, C.E. Synaptically released glutamate does not overwhelm transporters on hippocampal astrocytes during high-frequency stimulation. *J. Neurophysiol.* **83**, 2835–2843 (2000).
19. Heine, M. *et al.* Surface mobility of postsynaptic AMPARs tunes synaptic transmission. *Science* **320**, 201–205 (2008).
20. Arizono, M. *et al.* Receptor-selective diffusion barrier enhances sensitivity of astrocytic processes to metabotropic glutamate receptor stimulation. *Sci. Signal.* **5**, ra27 (2012).
21. Toulme, E. & Khakh, B.S. Imaging P2X4 receptor lateral mobility in microglia: regulation by calcium and p38 MAPK. *J. Biol. Chem.* **287**, 14734–14748 (2012).
22. Groc, L. & Choquet, D. Measurement and characteristics of neurotransmitter receptor surface trafficking (Review). *Mol. Membr. Biol.* **25**, 344–352 (2008).
23. Groc, L. *et al.* Differential activity-dependent regulation of the lateral mobilities of AMPA and NMDA receptors. *Nat. Neurosci.* **7**, 695–696 (2004).
24. Takeda, H., Inazu, M. & Matsumiya, T. Astroglial dopamine transport is mediated by norepinephrine transporter. *Naunyn Schmiedebergs Arch. Pharmacol.* **366**, 620–623 (2002).
25. Yang, Y. *et al.* Presynaptic regulation of astroglial excitatory neurotransmitter transporter GLT1. *Neuron* **61**, 880–894 (2009).
26. Genoud, C. *et al.* Plasticity of astrocytic coverage and glutamate transporter expression in adult mouse cortex. *PLoS Biol.* **4**, e343 (2006).
27. Benediktsson, A.M. *et al.* Neuronal activity regulates glutamate transporter dynamics in developing astrocytes. *Glia* **60**, 175–188 (2012).
28. Tardin, C., Cognet, L., Bats, C., Lounis, B. & Choquet, D. Direct imaging of lateral movements of AMPA receptors inside synapses. *EMBO J.* **22**, 4656–4665 (2003).
29. Groc, L., Choquet, D. & Chaouloff, F. The stress hormone corticosterone conditions AMPAR surface trafficking and synaptic potentiation. *Nat. Neurosci.* **11**, 868–870 (2008).
30. Dupuis, J.P. *et al.* Surface dynamics of GluN2B-NMDA receptors controls plasticity of maturing glutamate synapses. *EMBO J.* **33**, 842–861 (2014).
31. Marcaggi, P., Billups, D. & Attwell, D. The role of glial glutamate transporters in maintaining the independent operation of juvenile mouse cerebellar parallel fibre synapses. *J. Physiol. (Lond.)* **552**, 89–107 (2003).
32. Danbolt, N.C. Glutamate uptake. *Prog. Neurobiol.* **65**, 1–105 (2001).
33. Tzingounis, A.V. & Wadiche, J.I. Glutamate transporters: confining runaway excitation by shaping synaptic transmission. *Nat. Rev. Neurosci.* **8**, 935–947 (2007).
34. Rothstein, J.D. *et al.* Knockout of glutamate transporters reveals a major role for astroglial transport in excitotoxicity and clearance of glutamate. *Neuron* **16**, 675–686 (1996).
35. Yernool, D., Boudker, O., Jin, Y. & Gouaux, E. Structure of a glutamate transporter homologue from *Pyrococcus horikoshii*. *Nature* **431**, 811–818 (2004).
36. Oliet, S.H., Piet, R. & Poulain, D.A. Control of glutamate clearance and synaptic efficacy by glial coverage of neurons. *Science* **292**, 923–926 (2001).
37. Pannasch, U. *et al.* Connexin 30 sets synaptic strength by controlling astroglial synapse invasion. *Nat. Neurosci.* **17**, 549–558 (2014).
38. Omrani, A. *et al.* Up-regulation of GLT-1 severely impairs LTD at mossy fibre–CA3 synapses. *J. Physiol. (Lond.)* **587**, 4575–4588 (2009).
39. Melone, M., Bellesi, M. & Conti, F. Synaptic localization of GLT-1a in the rat somatic sensory cortex. *Glia* **57**, 108–117 (2009).
40. Choquet, D. & Triller, A. The dynamic synapse. *Neuron* **80**, 691–703 (2013).
41. Overstreet, L.S., Kinney, G.A., Liu, Y.B., Billups, D. & Slater, N.T. Glutamate transporters contribute to the time course of synaptic transmission in cerebellar granule cells. *J. Neurosci.* **19**, 9663–9673 (1999).
42. Ventura, R. & Harris, K.M. Three-dimensional relationships between hippocampal synapses and astrocytes. *J. Neurosci.* **19**, 6897–6906 (1999).
43. Kullmann, D.M., Erdemli, G. & Asztely, F. LTP of AMPA and NMDA receptor–mediated signals: evidence for presynaptic expression and extrasynaptic glutamate spill-over. *Neuron* **17**, 461–474 (1996).
44. Krugers, H.J., Hoogenraad, C.C. & Groc, L. Stress hormones and AMPA receptor trafficking in synaptic plasticity and memory. *Nat. Rev. Neurosci.* **11**, 675–681 (2010).
45. Mikasova, L. *et al.* Disrupted surface cross-talk between NMDA and Ephrin-B2 receptors in anti-NMDA encephalitis. *Brain* **135**, 1606–1621 (2012).
46. Rothstein, J.D., Van Kammen, M., Levey, A.I., Martin, L.J. & Kuncl, R.W. Selective loss of glial glutamate transporter GLT-1 in amyotrophic lateral sclerosis. *Ann. Neurol.* **38**, 73–84 (1995).
47. Tanaka, K. *et al.* Epilepsy and exacerbation of brain injury in mice lacking the glutamate transporter GLT-1. *Science* **276**, 1699–1702 (1997).
48. Scimemi, A. *et al.* Amyloid-beta1–42 slows clearance of synaptically released glutamate by mislocalizing astrocytic GLT-1. *J. Neurosci.* **33**, 5312–5318 (2013).
49. Liévens, J.C. *et al.* Impaired glutamate uptake in the R6 Huntington's disease transgenic mice. *Neurobiol. Dis.* **8**, 807–821 (2001).
50. Massie, A. *et al.* Time-dependent changes in GLT-1 functioning in striatum of hemi-Parkinson rats. *Neurochem. Int.* **57**, 572–578 (2010).

ONLINE METHODS

Cell culture and protein expression. Mixed cultures of hippocampal glia and neurons were prepared from E18 Sprague-Dawley rats following previously described methods[51,52]. Briefly, cells were plated at a density of 60×10^3 cells per ml on poly-L-lysine precoated coverslips. Cultures were kept in neurobasal medium (Invitrogen) with 3% horse serum (vol/vol, Invitrogen) for several days before changing to serum-free neurobasal medium (Invitrogen). Cultures were maintained at 37 °C in 5% CO_2 for 20 d *in vitro* at maximum. Cells were transfected at 7–10 d *in vitro* using Effectene transfection kit (Qiagen) with plasmids coding for Enhanced Green Fluorescent Protein (EGFP) and GLT-1^{flag}, a GLT-1 transporter with a flag tag (DYKDDDDK) inserted into the second extracellular loop of the protein between Pro^{199} and Pro^{200} (a gift from M. Rattray, University of Bradford)[53]. To label synapses, neurons were transfected with the postsynaptic protein Homer-dsRed before imaging.

Immunocytochemistry. For immunostaining, surface GLT-1^{flag} was stained using a monoclonal antibody to Flag (1 µg ml^{-1}; Sigma F2555) for 30 min on live mixed cultures at 37 °C and 5% CO_2. Cells were then fixed with 4% paraformaldehyde (PFA, vol/vol) for 15 min, washed and then incubated with appropriate secondary antibodies. For synapse labeling experiments, we used secondary goat antibody to mouse conjugated to Alexa-568 (1 µg ml^{-1}, 1 h; Molecular probes A11004). for GLT-1^{flag}. To label Shank, neurons were permeabilized using 0.1% Triton X-100 (vol/vol), incubated with a primary rabbit polyclonal antibody to Shank (1 µg ml^{-1}, 1 h; Abcam 138126) and finally incubated with secondary goat antibody to rabbit conjugated to Alexa-488 (2 µg ml^{-1}, 30 min; Molecular Probes A1008). For quantification of synaptic content, cells were transfected with Homer-dsRed before immunostaining for GLT-1^{flag} using a monoclonal antibody to FLAG antibody (1 µg/ml; Sigma F2555) for 30 min followed by a secondary goat antibody to mouse FITC (3 µg ml^{-1}; Invitrogen 62-6511) for 1 h. To quantify total GL-1 expression in transfected versus non-transfected astrocytes, cells were incubated for 30 min with antibody to FLAG (to tag transfected cells, 1 µg ml^{-1}; Sigma F2555) before fixation and labeling with antibody to GLT-1 that recognized an intracellular epitope (2 µg ml^{-1}; Millipore AB1783) and thus label all GLT-1 (both endogenous and exogenous). Cells were washed, mounted and preparations were kept at 4 °C until imaging. Fluorescent specimens were examined under a spinning disk confocal microscope (Leica DMI 6000B, Leica microsystems) equipped with appropriate lasers and excitation/emission filters, or with an epifluorescence microscope (Zeiss Axiophot, Carl Zeiss). Images were analyzed using Metamorph software (Universal Imaging).

COS cells. COS-7 cells were plated in 12 well plates at a density of 30,000 cells per well in Dulbecco's Modified Eagle's Medium (Invitrogen) supplemented with 1% glutamax (vol/vol, Gibco), 1% sodium pyruvate (vol/vol, Sigma-Aldrich) and 10% fetal bovine serum (vol/vol, Invitrogen). After 1 day, cells were transfected or not with GLT-1^{flag} using Lipofectamine 2000 (Invitrogen) and left under humidified 5% CO_2 atmosphere (37 °C) for 2 d before experimentation.

Single-particle (quantum dot) tracking and surface diffusion calculation. Single-particle (QD) labeling and microscopy was performed as previously described[54]. Briefly, hippocampal primary cultures were incubated for 10 min (37 °C) with monoclonal antibodies to FLAG epitope (10 µg ml^{-1}; Sigma F2555) to tag GLT-1^{flag} or DAT^{flag}. Cells were then washed and incubated for 10 min (37 °C) with quantum dots 655 goat F(ab′)2 antibody to mouse IgG (1 µg ml^{-1}; Invitrogen). For QD tracking of endogenous GLT-1 (GLT-1^{endo}), we used a rabbit polyclonal antibody to GLT-1 antibody which recognizes an extracellular epitope of the transporter (1 µg ml^{-1}; NBP1-20136, Novus Biologicals), followed by a QD 655 goat F(ab′)2 antibody to rabbit IgG (1 µg ml^{-1}; Invitrogen). Nonspecific binding was blocked by the addition of 1% casein or 1% BSA (vol/vol, Vector Laboratories) to the quantum dots 15 min before use. Cells were again rinsed and mounted in an aluminum chamber filled with artificial cerebrospinal fluid (aCSF) solution containing 115 mM NaCl, 1.5 mM KCl, 1.6 mM $CaCl_2$, 1.6 mM $MgCl_2$, 8.5 mM HEPES and 8.5 mM D-glucose; osmolarity was 250–260 mosmol kg^{-1}; pH 7.4. Images were acquired using a Nikon microscope (NIKON Eclipse TE2000-U) with the stage heated to 37 °C using an air blower (World Precision Instruments) and an objective heater (Bioptechs). Quantum dots were detected using a mercury lamp and appropriate excitation/emission filters. Images were obtained with an acquisition time of 50 ms with 1,000 consecutive frames. Signals were detected using an EM-CCD camera (Quantem, Roper Scientific). Quantum dots were followed on randomly selected astrocytes expressing GFP and tagged with GLT-1^{flag}. Quantum dot recording sessions were processed with the MetaMorph software (Universal Imaging). The instantaneous diffusion coefficient D was calculated for each trajectory, from linear fits of the first four points of the mean-square-displacement versus time function using $MSD(t) = <r^2> (t) = 4Dt$. The two-dimensional trajectories of single molecules in the plane of focus were constructed by correlation analysis between consecutive images using a Vogel algorithm. Synaptic dwell time was calculated for exchanging transporters and defined as the mean time spent in the synaptic area. The two-dimensional trajectories of single molecules in the plane of focus were constructed by correlation analysis between consecutive images using a Vogel algorithm.

For the different experimental conditions, drugs were added into the bath to see whether they had an effect on GLT-1 diffusion. The drugs applied were L-glutamate (100 µM, Sigma-Aldrich), TBOA (DL-threo-benzyloxyaspartate, 30 µM, Tocris), TTX (1 µM, Tocris), the glutamate receptor antagonist cocktail comprised AP5 (D-(−)-2-Amino-5-phosphonopentanoic acid, 10 µM, Tocris), NBQX (2,3-dioxo-6-nitro-1,2,3,4-tetrahydrobenzo[*f*]quinoxaline-7-sulfonamide, 10 µM, Tocris) and MCPG ((*RS*)-α-methyl-4-carboxyphenylglycine, 500 µM, Tocris).

MNI-caged L-glutamate uncaging. Uncaging experiments were carried out in mixed hippocampal cultures between 14–16 d *in vitro*. Cells were transfected with GLT-1^{flag} 24 h before uncaging experiments. On the day of experimentation, cells were incubated with primary and secondary antibodies for quantum dot trafficking before 30-s incubation with Mitotracker green (1:2,000, Molecular Probes) to mark mitochondria-rich synapses. Coverslips were imaged in aCSF solution containing 115 mM NaCl, 1.5 mM KCl, 1.6 mM $CaCl_2$, 1.6 mM $MgCl_2$, 8.5 mM HEPES and 8.5 mM D-glucose; osmolarity was 250–260 mosmol kg^{-1}; pH 7.4 with 5 mM MNI-caged L-glutamate (Tocris). Uncaging experiments were carried out on a Nikon Ti-Eclipse inverted microscope equipped with a stage heater at 37 °C (World Precision Instruments), a 100X objective and 405, 491, 561 and 642 nm lasers. Signals were detected using an EM-CCD camera (Quantem, Roper Scientific). Regions of interest (ROIs) were chosen arbitrarily at synapses in close apposition to GLT-1^{flag}–transfected astrocytes. Uncaging was performed using a single laser pulse at 405 nm on ROIs directly beside synapses, with a maximum pulse duration of 2 ms. Trajectories of GLT-1^{flag} tagged with QDs were analyzed as described above for a duration of 30 s before uncaging and 60 s directly after uncaging.

Stereotaxic injections. Surgical procedures were done in accordance with the guidelines of the ethical committee for animal research in Bordeaux University. Sprague-Dawley rats (male and female, P16-22) were anesthetized with isofluorane and mounted on a Kopf stereotaxic frame. The heads were placed in a surgical mask to maintain the skull stable. A constant flux of an isoflurane/air mixture was applied inside the surgical mask. 500–1,000 nl of either rabbit polyclonal antibodies directed against GLT-1 (NBP1-20136, Novus Biologicals) or goat antibody to rabbit IgG (0.4 µg µl^{-1}, Invitrogen A10533) were dissolved in a phosphate-buffered saline (0.1 M, pH 7.4) and infused into the dorsal hippocampus (coordinates relative to bregma, AP: −4.5 mm, ML: ±2.2 mm, DV: −2.5 mm at P17) using borosilicate micropipettes (GC150F-10, Harvard Apparatus) prepared with a vertical micropipette puller (PC-10, Narishige). The solution was injected in the hippocampus at approximately 250 nl min^{-1} using a Picospritzer (Parker Hannifin). After injection, the needle was left *in situ* for a few minutes to reduce reflux up the needle. The incision was both mechanically and chemically sutured. Rats were then allowed to recover before being used for slice electrophysiology experiments.

Cell culture. Spontaneous excitatory postsynaptic currents (sEPSCs) were recorded in whole-cell patch clamp (V_{hold} = −70 mV) from hippocampal neurons at 14–16 d *in vitro* located in the close proximity of GFP/GLT-1^{flag}–transfected astrocytes. All experiments were conducted under continuous perfusion of extracellular medium containing 145 mM NaCl, 2.5 mM KCl, 10 mM HEPES, 10 mM D-glucose, 2 mM $MgCl_2$, 2 mM $CaCl_2$, adjusted to pH 7.4 with NaOH. All chemicals were purchased from Sigma-Aldrich unless otherwise stated. The bath was heated to 32 °C using a temperature control system (Bad controller V, Luigs & Neumann) and was supplemented in $GABA_A$ and $GABA_B$ receptors antagonists SR95531 (10 µM, Tocris) and CGP55845 (5 µM, Tocris), respectively, in order to block inhibitory neurotransmission. Whole-cell recordings were performed using 1.5 mm external diameter borosilicate pipettes (GC150F-10, Harvard Apparatus)

prepared with a micropipette puller (P97, Sutter Instruments). Electrodes (3.5-5 MΩ) were filled with a solution containing 125 mM $CsCH_3SO_3$, 2 mM $MgCl_2$, 1 mM $CaCl_2$, 10 mM EGTA, 10 mM HEPES, 4 mM Na_2-ATP, 0.4 mM Na_3-GTP, 5 mM QX-314, adjusted to pH 7.25 with CsOH. Alexa-568 was added to the internal solution for further immunodetection.

Recordings were performed using a Multiclamp 700A amplifier and a Digidata 1322A interface controlled by Clampex 10.1 (Molecular Devices). Signals were sampled at 20 kHz and low-pass filtered at 2 kHz, respectively. sEPSC detection and analysis was performed using an in-house software (Detection Mini, M. Goillandeau). Access resistance and leak currents were monitored continuously and experiments were discarded if these parameters changed by more than 15% during recording.

Brain slices. P16–22 Sprague-Dawley rats (male and female) anesthetized with isoflurane and parasagittal brain slices (350 µm thick) were prepared in an ice-cold sucrose buffer solution containing 250 mM sucrose, 2 mM KCl, 7 mM $MgCl_2$, 0.5 mM $CaCl_2$, 1.15 mM NaH_2PO_4, 11 mM glucose and 26 mM $NaHCO_3$ (gassed with 95% O_2/5% CO_2). Slices were then incubated for 30 min at 33 °C and subsequently stored at 20–22 °C in an aCSF solution containing 126 mM NaCl, 3.5 mM KCl, 2 mM $CaCl_2$, 1.3 mM $MgCl_2$, 1.2 mM NaH_2PO_4, 25 mM $NaHCO_3$ and 12.1 mM glucose (gassed with 95% O_2/5% CO_2; pH 7.35). Whole-cell voltage-clamp recordings of CA1 pyramidal cells were performed using infrared differential interference contrast microscopy under continuous perfusion of heated aCSF (32 °C, except when stated for recordings performed at 20 °C) saturated with 95% O_2/5% CO_2. Electrodes (4–5 MΩ) were prepared from borosilicate pipettes (GC150T-10, Harvard Apparatus) with a vertical micropipette puller (PC-10, Narishige) and filled with a solution containing 120 mM cesium methanesulfonate, 4 mM NaCl, 4 mM $MgCl_2$, 10 mM HEPES, 0.2 mM EGTA, 4 mM Na_2ATP, 0.33 mM Na_3GTP and 5 mM phosphocreatine adjusted to pH 7.3 with CsOH. sEPSC were recorded using an EPC10 USB amplifier (HEKA Elektronik) at −70 mV in the presence of bicuculline (20 µM) to block $GABA_A$ receptors. Signals were sampled at 20 kHz and low-pass filtered at 2 kHz, respectively. sEPSC detection and analysis was performed using an in-house software (Detection Mini, M. Goillandeau). Access resistance and leak currents were monitored continuously and experiments were discarded if these parameters changed by more than 15% during recording.

For astrocyte glutamate transporter current recordings, brain slices (350 µm thick) were prepared in a choline chloride buffer solution containing 120 mM $C_5H_{15}ClNO$, 3 mM KCl, 2 mM $MgCl_2$, 0.6 mM $CaCl_2$, 1.25 mM NaH_2PO_4, 10 mM glucose and 26 mM $NaHCO_3$ (gassed with 95% O_2 / 5% CO_2; 296 mosmol kg^{-1}; pH 7.35). Slices were then incubated for 30 min at 33 °C and subsequently stored at 20–22 °C in aCSF solution containing 120 mM NaCl, 2.5 mM KCl, 2 mM $CaCl_2$, 1.3 mM $MgCl_2$, 1.25 mM NaH_2PO_4, 25 mM $NaHCO_3$ and 10 mM glucose (gassed with 95% O_2 / 5% CO_2; 296 mosmol kg^{-1}; pH 7.35). Astrocytes in CA1 stratum radiatum were first identified based on cell size (<10 µM) and shape. Whole-cell patch-clamp recordings were performed at 32 °C, with a flow of 3.5 ml min^{-1}, using pipettes (5–6 MΩ) pulled from borosilicate glass (1.5 mm o.d., Harvard Apparatus) and filled with a solution containing 124 mM $KMeSO_3$, 10 mM HEPES, 4 mM $MgCl_2$, 4 mM ATP, 0.4 mM GTP, 10 mM sodium creatine PO_4 (pH 7.2–7.3 adjusted with KOH; 292 mosmol kg^{-1}). Astrocytes were characterized by a low input resistance, a linear current voltage relationship using a ramp voltage command from −110 to +100 mV (600-ms duration) in voltage-clamp mode, and absence of action potentials (current steps) in current-clamp mode. This relationship was analyzed on-line using pClamp10 (Axon Instruments). For each experiment, the resting membrane potential was first recorded in current-clamp configuration and cells with resting potential >−70 mV were automatically rejected. Then, after a stable baseline, input/output relationship of field excitatory postsynaptic potentials (fEPSPs) recorded through the astrocyte was performed before going back to voltage clamp mode to record glutamate transporter currents. For synaptic stimulation experiments, Schaffer collaterals were stimulated (100 µs, 10–100 µA, 0.033 Hz) using a bipolar tungsten electrode placed in the stratum radiatum 300 µm away from the recording electrode. At the end of each experiment, synaptic activity–elicited astrocytic GLT-1–mediated currents were blocked using TBOA (DL-threo-benzyloxyaspartate, 50 µM; Tocris). For glutamate puff experiments, 200 µM of L-glutamate was puffed for 40 ms at 10 psi using a Picospritzer (Parker Hannifin) within approximately 70 µm of the cell of interest, as previously reported[55]. Glutamatergic receptors were inhibited using a cocktail of the AMPAR antagonist NBQX (10 µM), the NMDAR antagonist AP5 (50 µM), and the mGluR antagonists MPEP (2-methyl-6-(phenylethynyl)pyridine hydrochloride, 50 µM; Tocris) and/or MCPG ((*RS*)-α-Methyl-4-carboxyphenylglycine, 500 µM; Tocris) when specified. Recordings were acquired using a Multiclamp 700B amplifier (Axon Instruments), digitized at 20 kHz and filtered at 2 kHz.

^{3}H-glutamate uptake. ^{3}H-glutamate uptake assays were performed on either COS-7 cells or mixed hippocampal cell cultures (astrocytes and neurons). Incubations with radiolabeled glutamate were performed in HEPES-buffered saline (HBS) solution (5 mM Tris base, pH 7.4, 10 mM HEPES, 140 mM NaCl, 2.5 mM KCl, 1.2 mM $CaCl_2$, 1.2 mM $MgCl_2$, 1.2 mM K_2HPO_4, 10 mM glucose) supplemented with 50 µM L-glutamate. Cells were washed twice with Na^+-free HBS solution (prepared by equimolar replacement of Na^+ with choline) at 37 °C then incubated with normal HBS (containing 50 µM ^{3}H-glutamate at 1 µCi ml^{-1}) at 37 °C for 6 min. Assays were stopped by aspiration of HBS (containing ^{3}H-glutamate) followed by two washes with ice-cold Na^+-free HBS and dishes were also placed on ice. Cells were then lysed in 0.1 M NaOH and accumulated radioactivity measured by liquid scintillation. K_m and V_{max} were determined from the saturation data using increasing concentrations of glutamate. A minimum of three independent experiments were performed for each condition.

Acid wash. To investigate how long GLT-1^{flag} stays at the surface of a cell, we used an acid wash protocol[56]. For acid wash experiments, we used a low pH (pH 2) aCSF of the same composition as for live QD imaging at 4 °C. Mixed hippocampal cultures, transfected with GLT-1^{flag} were incubated for 10 min (37 °C) with monoclonal antibodies to flag epitope (10 µg ml^{-1}; Sigma F2555) to tag GLT-1^{flag}. Cells were then washed and incubated for 10 min (37 °C) with quantum dots 655 goat F(ab')2 antibody to mouse IgG (1 µg ml^{-1}; Invitrogen). Following this step, cells were imaged in exactly the same manner as for QD imaging (1,000 frames, 50 ms per frame acquisition) and cells were left for 10-, 15-, 20- and 30-min intervals before a 1-min acid wash (incubation with a low pH, cold aCSF, pH 2, 4 °C) to break antibody-protein bonds and so the only transporters with QDs still attached are the ones that have been internalized. This acidic aCSF was then removed and replaced with normal aCSF (pH 7.4, 37 °C) and another QD imaging series was acquired. Total numbers of trajectories were compared in before and after acid wash at different time points to assess the internalization of GLT-1^{flag}-QD complexes during these specific time periods.

Data and statistical analysis. For all experiments, recorded cells were randomly selected, and animals that received injections were also randomly assigned to any experimental conditions. There was no blinding in our data collection. All statistical tests were carried out using GraphPad Prism 4.0. Data are presented as mean ± s.e.m. or median ± IQR. Normally distributed data sets were compared using parametric tests (as indicated in **Supplementary Table 1**). Data not distributed normally were compared using the appropriate non-parametric tests. All tests were two-sided. Paired two-tailed Student's *t* tests, two-tailed Mann-Whitney tests and one-way analysis of variance tests (with appropriate *post hoc* tests; indicated in **Supplementary Table 1**) were used for all statistical analysis. No statistical tests were carried out to predetermine sample sizes, but our sample sizes are comparable to those previously reported in the literature[51,57–59].

A **Supplementary Methods Checklist** is available.

51. Groc, L. *et al.* Differential activity-dependent regulation of the lateral mobilities of AMPA and NMDA receptors. *Nat. Neurosci.* **7**, 695–696 (2004).
52. Bard, L. *et al.* Dynamic and specific interaction between synaptic NR2-NMDA receptor and PDZ proteins. *Proc. Natl. Acad. Sci. USA* **107**, 19561–19566 (2010).
53. Peacey, E., Miller, C.C., Dunlop, J. & Rattray, M. The four major N- and C-terminal splice variants of the excitatory amino acid transporter GLT-1 form cell surface homomeric and heteromeric assemblies. *Mol. Pharmacol.* **75**, 1062–1073 (2009).
54. Groc, L. *et al.* Surface trafficking of neurotransmitter receptor: comparison between single-molecule/quantum dot strategies. *J. Neurosci.* **27**, 12433–12437 (2007).
55. Bergles, D.E. & Jahr, C.E. Synaptic activation of glutamate transporters in hippocampal astrocytes. *Neuron* **19**, 1297–1308 (1997).
56. Tardin, C., Cognet, L., Bats, C., Lounis, B. & Choquet, D. Direct imaging of lateral movements of AMPA receptors inside synapses. *EMBO J.* **22**, 4656–4665 (2003).
57. Tong, G. & Jahr, C.E. Block of glutamate transporters potentiates postsynaptic excitation. *Neuron* **13**, 1195–1203 (1994).
58. Heine, M. *et al.* Surface mobility of postsynaptic AMPARs tunes synaptic transmission. *Science* **320**, 201–205 (2008).
59. Mennerick, S. & Zorumski, C.F. Glial contributions to excitatory neurotransmission in cultured hippocampal cells. *Nature* **368**, 59–62 (1994).

doi:10.1038/nn.3901